Turbulence modification by large-scale organized electrohydrodynamic flows

Alfredo Soldati[a)]
Centro Interdipartimentale di Fluidodinamica e Idraulica and Dipartimento di Scienze e Tecnologie Chimiche, Università degli Studi di Udine, Via Cotonificio 108, 33100 Udine, Italy

Sanjoy Banerjee
Department of Chemical Engineering, University of California at Santa Barbara, Santa Barbara, California 93106

(Received 11 August 1997; accepted 13 March 1998)

The interactions of flows generated by ionic discharges with wall turbulence are not only of interest for turbulence control, but also for devices of industrial importance, such as wire-plate electrostatic precipitators (ESPs). Under conditions of uniform discharge, in wire-plate ESPs, arrays of regular, spanwise vortices are found in the absence of a through-flow. These arise from ionic discharges from the spanwise wires placed between the grounded plates on each side. The interactions of such electrohydrodynamic (EHD) flows with a turbulent through-flow are still poorly understood. Direct numerical simulation (DNS) is an attractive method for investigating such problems since the details of the interactions can be unraveled, and the results are directly applicable to industrial-scale systems because their Reynolds numbers are typically quite low. In this study, pseudospectral channel flow simulations were performed with the electrohydrodynamic effects being modeled by a spatially varying body-force term in the equations of fluid motion. The interactions between EHD flows and wall structures were elucidated by examining the instantaneous structure of the flow field. Results indicate that the mean flow, the EHD flows, and the turbulence field undergo significant modifications caused by mutual interaction. First, it is found that EHD flows reduce drag, allowing larger flow rates for a given pressure drop. Second, the EHD flows themselves appear weakened by the presence of the through-flow, particularly in the central region of the channel. The EHD flows affect the turbulence field by both increasing dissipation and turbulence production, the overall turbulence level being determined by the balance between the increased dissipation and production. Even though high EHD flow intensities may increase streamwise and wall-normal turbulence intensities, the Reynolds stress is reduced, consistent with the observed reduction in drag. From a mechanistic viewpoint, there are indications that EHD flows of the type investigated here reduce drag by decreasing the relative importance of the positive Reynolds stress contributions, i.e., second (ejections) and fourth (sweeps) quadrant events, compared to the negative Reynolds stress contributions, i.e., first and third quadrant events. © *1998 American Institute of Physics.* [S1070-6631(98)01707-3]

I. INTRODUCTION

When a potential difference is applied across a fluid in which ionic species are dispersed, the ions drift under the action of the Coulomb force, and interact with fluid molecules. As a result of such interactions, ions exchange momentum with the fluid, so that ''electrohydrodynamic'' (EHD) fluid motions are generated. For certain body-force distributions, EHD flows form arrays of large-scale, spanwise, counter-rotating vortical structures, as shown in Fig. 1. The superposition of this periodic structure onto wall turbulence leads to turbulence modification. Such flows are not only of interest as a means of controlling turbulence but also from a practical viewpoint as they arise in wire-plate electrostatic precipitators (ESPs).

The scenario shown in Fig. 1, with an array of counter-rotating EHD-generated vortices superimposed onto a turbulent through-flow, is typical of wire-plate ESPs, which consist of a duct with vertical walls through which a gas, bearing suspended particles, is driven by a pressure gradient. Wire electrodes (usually vertical and equispaced) are placed along the duct centerline and are kept at a potential well above the threshold for ionic discharge. The ions released into the flow are driven toward the grounded walls by the action of the electrostatic field. A sketch of the flow configuration is shown in Fig. 2. Ions streaming across the flow interact with initially neutral air-borne particles and charge them. These ions interact with fluid particles and generate EHD flows. From a macroscopic point of view, EHD flows appear to arise from the action of the Coulomb force. Background material on electrohydrodynamic convection may be found in earlier studies.[1,2]

Electrostatic forces, alone or together with magnetic

[a)]Author to whom correspondence should be addressed. Electronic mail: alfredo@euterpe.dstc.uniud.it

 © 1998 American Institute of Physics

Downloaded 20 Jun 2001 to 158.110.50.27. Redistribution subject to AIP license or copyright, see http://ojps.aip.org/phf/phfcr.jsp

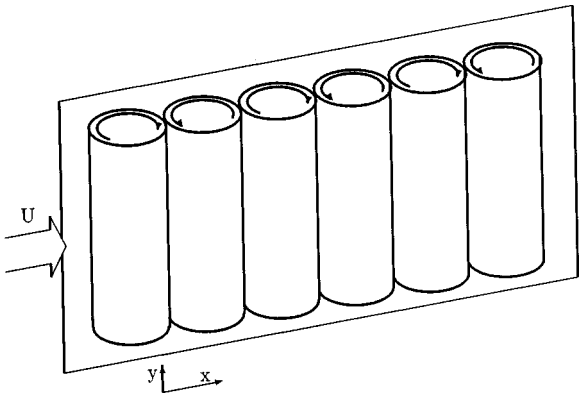

FIG. 1. Schematic representation of an array of large-scale spanwise vortical structures typical of wire-plate electrostatic precipitators.

forces, are currently one of the possible choices to reduce drag and control turbulence structure.[3,4] In wire-plate ESPs, electrostatic forces are required to separate air-borne particles and were considered to have a negative effect on drag because turbulence might be increased. In this paper, we directly simulate the flow in an ESP, albeit at a somewhat lower Reynolds number, and obtain quantitative estimates of effects on drag, various turbulence statistics and transport coefficients. More broadly, the possibility of controlling turbulence parameters by such superimposed EHD flows is identified.

In wire-plate precipitators, the characteristics of EHD flows depend on the distribution of the body force which, in turn, depends on the distribution of space charge and the electrostatic field. If ionic discharge occurs uniformly along the wires, the distribution of the body force is two-dimensional in x and z, as shown in Fig. 3(a). This figure illustrates the body force generated by two wire electrodes: the distribution has a center of symmetry at the wire and shows a periodic, celllike pattern. The application of such a body force to still fluid generates the two-dimensional recirculating flows shown in Fig. 3(b). It can be seen that planar jets are directed from the wires toward the grounded walls

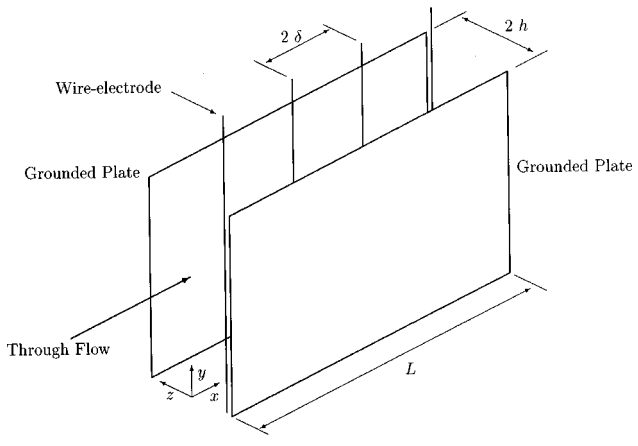

FIG. 2. Schematic of a wire-plate precipitator. A view of the computational domain: the channel, in the middle of which four wire electrodes are placed, is delimited by two vertical walls.

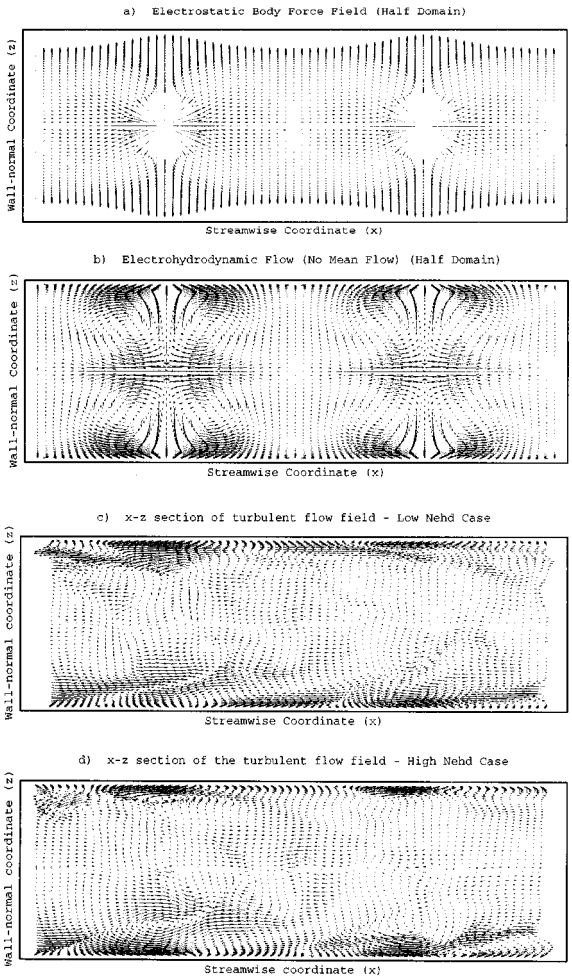

FIG. 3. Electrostatic body force distribution and generation of electrohydrodynamic vortices in still and turbulent flow in the cross section $(x-z)$. Figure refers to half-domain, containing two wires. (a) Two-dimensional distribution of the electrostatic body force; (b) $N_{\mathrm{EHD}}=\infty$, two-dimensional configuration of EHD jets and recirculating flows in still fluid: the body force generates four equal vortical structures, two upstream and two downstream from each wire; (c) Low N_{EHD}, instantaneous distribution of the fluctuating velocity field in the $x-z$ plane; (d) High N_{EHD}, instantaneous distribution of the fluctuating velocity field in the $x-z$ plane; The well organized nature of the recirculating structures in the no-flow case is partially lost when a through-flow is imposed. The recirculating structures are visible, mostly in the wall region, indicated by the upstream and downstream flows due to impingement of jets on the wall. Recirculating flows are stronger for the high N_{EHD} case.

and, by continuity, return flows are directed toward the center of the channel. In response to the celllike distribution of the body force, EHD flows also show a celllike pattern, four vortical structures being generated by each wire. The existence of such two-dimensional vortical flows in still fluid has been reported by a number of authors both in experimental[5,6] and theoretical[5,7–9] studies.

In ESPs, either a positive or a negative potential may be applied to the wire electrodes, depending on the type of particles to be collected. A positive discharge is usually distributed uniformly along the wire. As a consequence, the distribution of the body force is two-dimensional in x and z. A negative discharge on the other hand is more unstable at low potential, and ions are emitted from *tufts* which come and go,

Downloaded 20 Jun 2001 to 158.110.50.27. Redistribution subject to AIP license or copyright, see http://ojps.aip.org/phf/phfcr.jsp

and move along the wire generating a three-dimensional, fluctuating, body-force distribution.[10] At high potential, negative discharges also stabilize and tend to generate a two-dimensional field.

In the past, EHD flows generated by both negative and positive discharge have been investigated in various studies which aimed to characterize the fluid dynamic aspects of wire-plate precipitators. Most of this work is experimental,[11–15] or based on two-dimensional $k-\epsilon$ turbulence models.[15,16] The experiments indicate that uniform discharges increase turbulence slightly[11,15] or, under certain conditions, decrease turbulence intensity,[11] and that tuft discharges (negative discharges) increase turbulence intensity.[11,12,15]

Experiments have been done using hot-wire anemometry and laser Doppler anemometry (LDA), both of which have shortcomings as discussed below.

Hot-wire anemometry was used by Leonard *et al.*[11] and by Davidson and Shaughnessy,[12] who were aware that hot-wire anemometry could not be employed close to the wires because of current flowing to the probe. These authors, therefore, took all measurements well downstream of the last discharging wire (about three duct-widths downstream), and thus observed the flow where the effect of the electrohydrodynamic forces had decayed. Leonard *et al.*[11] measured mean velocity and intensity of the streamwise turbulent fluctuations both for negative and positive discharge using a grid to generate a homogeneous turbulence field upstream of the wires. They reported no variation in the mean velocity profile and an increase in turbulence intensity for negative discharge. For positive discharge, they found a decrease in turbulence intensity in the center of the channel, and an increase in the wall region.

Davidson and Shaughnessy[12] analyzed a laminar-turbulent transitional flow interacting with EHD flows generated by a negative discharge, measuring mean velocity and both cross-stream and streamwise turbulence intensities. They report no modification to the mean flow profile and a marked increase in the level of fluctuations. They also found a significant increase in the characteristic dimension of the flow structures.

Two component LDA was used by Kallio and Stock[15] and by Riehle and Löffler.[17] Even though LDA allows measurements to be made in the wire section (where it is vital to understand the flow field), the data measured are for the velocity of the *seed* particles, and not for the velocity of the fluid. The seed were aerosol droplets (usually about 1–6 μm in diameter) which behave like the pollutant particles to be separated in ESPs. They quickly become charged and drift significantly. As a consequence, estimates of the fluid velocity from these data are questionable. Using this technique, Kallio and Stock[15] measured turbulence intensity in two directions for both positive and negative discharge and reported an increase of turbulence dependent on the intensity of the undisturbed EHD flows. The increase was smaller for positive discharge. Similar results were obtained by Riehle and Löffler.[17]

Numerical calculations for the flow field in wire-plate ESPs were performed by Bernstein and Crowe[16] and by Kallio and Stock.[15] In both papers, a two-dimensional $k-\epsilon$ model was used and the resulting system of equations was solved using finite difference approximations. The results, of limited interest if the detailed flow structure is required, show the presence of EHD recirculating flows superimposed on the mean turbulent field. Clearly, there are questions about such calculations, as any possible *direct* contribution to the turbulence kinetic energy or dissipation rate from the electrohydrodynamic flows was ignored.

Beside these quantitative estimates of the turbulent flow field, attempts have been made to visualize the flow by photographing flow streaklines tagged with smoke[11,18] or small titanium particles.[14] Again, in such techniques, the behavior of the tracer is influenced by the Coulomb force. Nonetheless, the visualizations demonstrated the existence of steady EHD jets impinging on the walls and generating vortical structures. In some investigations performed with higher body force intensity,[14] the EHD flows were clear enough to characterize, even though they were distorted by the turbulent through-flow.

Considering again the periodic array of vortical structures superimposed onto wall turbulence, previous research indicates that the turbulent through-flow distorts their shape, and suggests that turbulence intensities are also modified. However, all experiments have been performed in facilities of rather short streamwise extent, and measurements were in the region of developing flow. Furthermore, because experimental measurements of the flow field are difficult to interpret due to direct coupling of the motion of seed particles to the electrostatic field through the Coulomb drift, the results must be regarded as qualitative at best. In particular, questions about effects on drag, turbulence structure and particle transport mechanisms are still unanswered.

The work presented here is to the best of our knowledge the first three-dimensional time-dependent solution of the fully developed turbulent channel flow interacting with the large-scale EHD spanwise vortical structures shown in Fig. 1. The direct solution of the governing equations for fluid motion was obtained by a pseudospectral solver, previously used for open channel[19] and closed channel flows.[20,21] Body-force distributions, which are governed by a set of Maxwell equations, were calculated using a finite difference scheme.[22]

The effect of EHD flows was investigated for one low, and one high, intensity level of the electrostatic body force, and a previous channel flow simulation, without EHD effects, at the same shear Reynolds number[20] was used as a reference for comparison purposes. The flow field was examined by a triple decomposition discussed later, in order to separate the mean field from the organized EHD field, and both from the turbulence field.

II. NUMERICAL SIMULATION OF EHD FLOWS AND WALL TURBULENCE IN A DUCT

Figure 2 shows a schematic of the precipitator through which the flow field was numerically simulated for an imposed pressure gradient. The fluid is air, assumed to be incompressible, Newtonian, with no-slip conditions at walls, and driven by a pressure gradient. The wire electrodes were

Downloaded 20 Jun 2001 to 158.110.50.27. Redistribution subject to AIP license or copyright, see http://ojps.aip.org/phf/phfcr.jsp

kept at a potential sufficient to ensure ionic discharge and the presence of distributed ionic species in the duct. Ions are subjected to the Coulomb force,[23] **F**, which may be expressed as

$$\mathbf{F}=\rho_c\mathbf{E}, \tag{1}$$

where ρ_c is the charge density and **E** is the electric field vector. They are driven toward the walls. In this process, the ions collide with fluid molecules, transferring momentum to them. This is equivalent to a body force which acts directly *on the fluid*.[24] Therefore, the equation of fluid motion in dimensional terms is

$$\rho\left[\frac{\partial u_i}{\partial t}+u_j\frac{\partial u_i}{\partial x_j}\right]=-\frac{\partial \mathscr{P}}{\partial x_i}+\mu\frac{\partial^2 u_i}{\partial x_j\,\partial x_j}+F_i, \tag{2}$$

where u_i are the dimensional velocity components along the three directions x_i (with x_1 being streamwise, x_2 being spanwise, and x_3 being the wall-normal directions), $\mathscr{P}$ is pressure, and ρ and μ are fluid density and dynamic viscosity, respectively. For the case under consideration, the body force depends only on x and z, implying that the body-force distribution does not fluctuate because of ionic convection. This is a realistic assumption, since ions have a drift velocity of about 100 m/s in air while the mean flow velocity is about 1 m/s. For liquids,[6,25] ionic convection may not be negligible in some situations and a ''two-way'' coupling will exist between the flow field and the electrostatic body force field. Here the coupling is ''one-way,'' i.e., the fluid does not modify the electrostatic body forces.

A. Flow field

The flow field was calculated by integrating the mass and momentum balance equations in dimensionless form obtained using the duct half-width, h, and the shear velocity, u_τ, defined as

$$u_\tau=\sqrt{\frac{\tau_w}{\rho}}, \tag{3}$$

where τ_w is the shear at the wall. Therefore, the mass and momentum balance equations in dimensionless form are

$$\frac{\partial u_i}{\partial x_i}=0, \tag{4}$$

and

$$\frac{\partial u_i}{\partial t}=-u_j\frac{\partial u_i}{\partial x_j}+\frac{1}{\mathrm{Re}}\frac{\partial^2 u_i}{\partial x_j\,\partial x_j}-\frac{\partial p}{\partial x_i}+\delta_{1,i}+\Phi_i, \tag{5}$$

where u_i is the ith component of the dimensionless velocity vector, $\delta_{1,i}$ is the mean dimensionless pressure gradient, Φ is the dimensionless electrostatic body force, and $\mathrm{Re}=hu_\tau/\nu$ is the shear Reynolds number. Equations (4) and (5) were solved directly using a pseudospectral method similar to that used by Kim *et al.*[26] to solve the turbulent, closed-channel flow problem and by Lam and Banerjee[19] to solve the turbulent, open-channel flow problem. The difference is the inclusion of the space dependent body force which, being steady and uncoupled to the flow field, was calculated once at the beginning of each simulation. If the body force term is treated together with the nonlinear terms, Eq. (5) may be recast as

$$\frac{\partial u_i}{\partial t}=S_i+\frac{1}{\mathrm{Re}}\frac{\partial^2 u_i}{\partial x_j\,\partial x_j}-\frac{\partial p}{\partial x_i}, \tag{6}$$

which is formally identical to the momentum equation solved by both Kim *et al.*[26] and Lam and Banerjee[19] and where S_i now includes the convective term, the mean pressure gradient, and the Coulomb term. The pseudospectral method is based on transforming the field variables into wave number space, using Fourier representations for the streamwise and spanwise directions and a Chebyshev representation for the wall-normal (nonhomogeneous) direction. A two level, explicit, Adams–Bashforth scheme for the nonlinear terms S_i, and an implicit Crank–Nicolson method for the viscous terms, were employed for time advancement. Details of the method have been published previously.[19]

With the duct dimensions shown in Fig. 2, air density of 1.38 kg/m^3, and air kinematic viscosity of 16.6×10^{-6} m^2/s, the shear velocity is 8.964×10^{-2} m/s, and the shear Reynolds number is equal to 108. For the reference case with no EHD effects,[20] the mean velocity is 1.16 m/s and the Reynolds number based on mean velocity and duct width is $\sim$2795. The velocity is in the range found in industrial and laboratory electrostatic precipitators.

B. The electrostatic body force

The electrostatic potential distribution and space charge distribution are given by the following set of equations:

$$\frac{\partial^2 V}{\partial x_i^2}=-\frac{\rho_c}{\epsilon_0}, \tag{7}$$

$$\rho_c^2=\epsilon_0\frac{\partial \rho_c}{\partial x_i}\frac{\partial V}{\partial x_i}=-\epsilon_0\frac{\partial \rho_c}{\partial x_i}E_i, \tag{8}$$

$$E_i=-\frac{\partial V}{\partial x_i}, \tag{9}$$

$$J_i=-\rho_c\beta E_i, \tag{10}$$

where, ϵ_0 is air permittivity ($\epsilon_0=8.854\times10^{-12}$), and $\beta=1.4311\times10^{-4}$ m^2/V s is ionic mobility[27] for positive discharge in air. An analytical solution for these equations may be obtained by assuming a uniform distribution of the space charge. The Poisson equation may then be reduced to a Laplace equation by a simple transformation.[7]

In the present case, Eqs. (7)–(10) were solved by a two-dimensional finite difference scheme, which has been widely used to calculate the two-dimensional Coulomb force distribution, due to positive discharge, in electrostatic precipitators.[5,9,22] Briefly, the scheme is based on an initial guess for the space charge density at the wire followed by iterative solution of Eqs. (7) and (8) until convergence of the plate current density is obtained.

The solution of the set of Eqs. (7)–(10) determines the spatial distribution of the body force [an example of such a distribution is shown in Fig. 3(a)].

Downloaded 20 Jun 2001 to 158.110.50.27. Redistribution subject to AIP license or copyright, see http://ojps.aip.org/phf/phfcr.jsp

C. Simulations of the flow field

Various parameters were chosen so as to obtain electrohydrodynamic conditions similar to those used in practice, and in previous investigations. A nondimensional number enters the problem, representing the ratio between the electrostatic body force and inertial forces acting on a fluid parcel.[5,11,12] This is called electrohydrodynamic number, N_{EHD}. In Leonard *et al.*,[11] and in this paper,

$$N_{\mathrm{EHD}}=\frac{i}{l\rho\beta U^2}, \tag{11}$$

where i represents the total current at the plate, l the length of the wire, and U the mean flow velocity. In the limiting case of $N_{\mathrm{EHD}}=0$, the flow is unaffected by electrohydrodynamic forces (i.e., it is channel flow). In the limiting case $N_{\mathrm{EHD}}=\infty$, the through-flow does not affect EHD flows, as shown in Fig. 3(b). In the present investigation, two different simulations were run, one with low N_{EHD} and the other with high N_{EHD}. The mean flow velocity is expected to vary depending on the value of the electrostatic body force. Thus it was not possible to identify *a priori* the value for the N_{EHD}. However, using the mean velocity calculated in the reference channel-flow case, the low N_{EHD} is about 1 and the high N_{EHD} is about 2.8. The effect of N_{EHD} is clearly evident from Figs. 3(c) and 3(d), where the fluctuating velocity field in the plane perpendicular to the wires is shown for the low and high N_{EHD} cases, respectively. The values for N_{EHD} in the present simulations are in the range used in previous work, e.g., Kallio and Stock[15] used N_{EHD} from 0.6 to ~ 8, Leonard *et al.*[11] used N_{EHD} from 0 to 2.4. This range is representative of actual electrostatic precipitators. For the low intensity case, the linear current density at the plate was $I_1=0.3\times10^{-3}$ A/m, with a potential at the wire of $V_1=32\,000$ V. In the high intensity case, the linear current density at the plate was $I_1=0.75\times10^{-3}$ A/m, with a potential at the wire of $V_1=42\,000$ V. Again, these values are typical of industrial electrostatic precipitators. From the fluid motion viewpoint, the wires are not taken into consideration, as they are usually rather fine and wake effects will be small in comparison with EHD effects. In typical laboratory conditions, the cylinder Reynolds number of the wire electrodes was found to vary from about 40, as in Kallio and Stock,[15] up to about 400, as in Davidson and Shaughnessy.[12] Wake effect may therefore be expected when no electrostatic field is applied. However, once the electrostatic potential is applied to the wires, the wake is no longer noticeable:[28] The flow around the wire is dominated by EHD flows, and wake effects become negligible.

Since the pressure gradient was maintained constant for the simulations, the shear Reynolds number was equal to 108 for both simulations and equal to a previous DNS of turbulent channel flow without EHD effects run by Soldati *et al.*[20] That simulation was assessed against experimental data[29,30] and other DNS[26] and is also used here as a reference to clarify modifications to the flow field produced by the EHD flows. Simulations presented here were run with $128\times64\times65$ nodes in a box of dimensionless size $1357\times678\times216$ in wall units (dimensionless variables in wall units are indicated by the superscript $+$) and a timestep $\Delta t^+=0.038$. This gives a resolution of $\Delta x_1^+=10.6$, $\Delta x_2^+=10.6$, and Δx_3^+ ranging from 0.13 next to the walls to 5.3 in the center of the channel. Such resolution is comparable with that of well known DNS databases.[26,31,32]

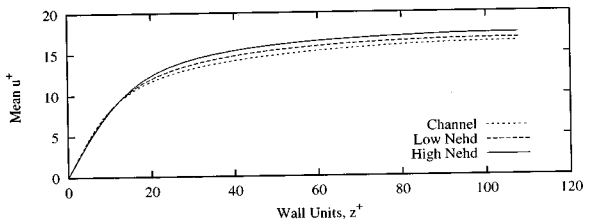

FIG. 4. Mean velocity of flow in the duct for channel flow, for low N_{EHD}, and for high N_{EHD}.

For both cases, the simulations were started from the steady turbulent channel flow computed in Soldati *et al.*[20] by turning on the electrostatic body force.

When the flow field become statistically steady, the results were stored for a sufficient number of time steps to allow reliable calculations of the turbulence statistics and the energy budget. It was not possible to directly evaluate the accuracy of the present simulations because of the lack of sufficiently reliable experimental results, as discussed in the introduction. An indication of the accuracy of the simulation is given by the maximum residual of the continuity equation computed at the nodes, which was always below $\epsilon=10^{-12}$ in wall units.

III. RESULTS

A. Mean quantities: drag reduction due to EHD flows

EHD flows generate no mean flow directly. Since they modify the turbulence field, influencing turbulent transfer mechanisms, mean flow variables may be expected to vary. To obtain correct values for the mean variables, averages must be obtained both in time and in the homogeneous directions (i.e., averaged over the $x-y$ plane). In Fig. 4, the mean velocity profile calculated for the low and high N_{EHD} cases is compared with that of turbulent channel flow.[20] The mean velocity increases, indicating a discernible drag reduction in the higher N_{EHD} case (note that the wall shear stress is held constant in the simulations, so an increase in mean velocity indicates drag reduction). Profiles are very similar in the wall region, the channel flow profile being slightly steeper, but they differ in the asymptotic value. The mean velocity in channel flow is about 1.16 m/s: It increases to 1.19 m/s ($\sim3\%$) in the low N_{EHD} case and up to 1.23 m/s ($\sim6\%$) in the high N_{EHD} case. Thus the value of the N_{EHD} number is 1.1 in the low intensity case and 2.5 in the high intensity case, and the Reynolds number based on mean velocity and duct width is ~2857 in the low N_{EHD} case and 2964 in the high N_{EHD} case. As drag varies approximately as the square of the mean velocity, the low N_{EHD} case results in $\sim6\%$ drag reduction, whereas in the high N_{EHD} case the reduction is $\sim12\%$.

Downloaded 20 Jun 2001 to 158.110.50.27. Redistribution subject to AIP license or copyright, see http://ojps.aip.org/phf/phfcr.jsp

Since EHD forces do not generate mean through-flow directly, in previous work,[12,15] attention was not paid to differences in the mean through-flow for a given pressure gradient.

B. Instantaneous structure of the flow field

The instantaneous structure of the fluctuating velocity field in the $x-z$ plane is shown in Figs. 3(c) and 3(d) for the low and the high N_{EHD} cases, respectively, for the distribution of the electrostatic body force shown in Fig. 3(a). As expected, recirculating structures show up more clearly in the high N_{EHD} case. Visualizations of the streaklines by Davidson and McKinney[14] for $N_{\mathrm{EHD}}=5.6$ show the presence of distinct vortical patterns superimposed on the turbulent field. In the present cases, however, N_{EHD} is lower and the EHD flows are not strong enough to prevent distortion of the vortices by the through-flow. The presence of EHD induced jetlike structures impinging on the wall are clearly evident from the upstream and downstream flows near the stagnation points, which appear to be located slightly downstream of the wires in both high and low N_{EHD} cases owing to mean flow advection.

In Figs. 3(c) and 3(d), regions of strong backflows appear upstream from the stagnation points because of the deflection of EHD ''jets'' after they impinge on the wall. These regions reach up to the wall and are expected to influence the undisturbed structure of the streamwise fluctuating velocity in the proximity of the walls. Figures 5(a), 5(b), and 5(c) illustrate the $x-y$ section at $z^+=4$ of the fluctuating streamwise velocity in a turbulent channel flow without EHD effects, in the low N_{EHD} case and in the high N_{EHD} case, respectively. In Fig. 5(a) streaky structures, which have been extensively studied for wall turbulence, even though their dynamics and generation mechanisms are still unclear,[32–34] show up clearly. However, it is clear that their pattern is affected by the presence of the four pairs of counter-rotating vortical structures, as evident from spanwise pattern superimposed on the streaky structures. This effect is more pronounced for higher N_{EHD}.

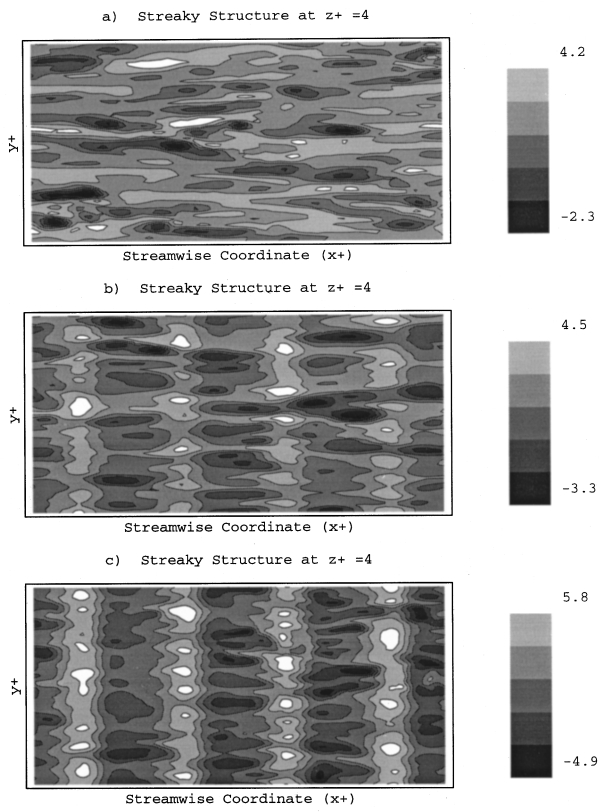

FIG. 5. Wall parallel $(x-y)$ section of the streamwise velocity component of the fluctuating field. Streaky structures in the near-wall region at $z^+=4$, for: (a) channel flow; (b) low N_{EHD} case; (c) high N_{EHD} case. Low (dark) and high (light) speed regions are clearly visible. The shading indicates the values of the dimensionless streamwise component of the velocity field in wall units. The influence of EHD flows is more clear for higher N_{EHD}.

C. Triple decomposition: Filtering of the flow field

EHD vortices are organized coherent structures. In order to separate the effect of these organized spanwise vortices from the turbulent flow field, and to clarify the role of EHD flows on turbulence modification, field variables, $f(x,y,z,t)$, were decomposed as

$$f(x,y,z,t)=\overline{f}(z)+\widetilde{f}(x,z,t)+f'(x,y,z,t), \tag{12}$$

where

$$\widetilde{f}=\langle f\rangle-\overline{f},$$

and $\overline{f}$ is the space average over the homogeneous directions (x and y), $\langle f\rangle$ is the phase average (the average over the spanwise direction in the present case), representing the organized EHD field, and f' is the instantaneous turbulent fluctuation. Similar decompositions have been applied previously to investigate the influence of an organized wave on a turbulent channel flow[35,36] and in discussions related to coherent structures in turbulent flows.[37]

D. Filtered EHD flows

In Fig. 6, the organized component of the flow field, $\tilde{v}$, is shown for the low and high N_{EHD} cases in a portion of the domain containing two wires—i.e., half of the computational domain. The recirculating structure of the EHD flows is evident, although the shape of the cells is distorted if compared to the undisturbed case of Fig. 3(b), corresponding to $N_{\mathrm{EHD}}=\infty$, which is included as a benchmark. The through-flow weakens the EHD flow, especially in the central region of the channel. Strong streamwise flows appear in the wall region beside the stagnation points. A more detailed picture of the shape of the vortical EHD cells may be had from the streamline plots in Fig. 7, where a portion of the domain again containing two wires is shown. Consider the no-flow case: each wire generates four equal vortical cells, two upstream and two downstream from the wire. For decreasing N_{EHD}, the vortical cells lose coherence, and intensity, and fluctuate in shape. In previous work,[9] oscillations of the vortical cells

Downloaded 20 Jun 2001 to 158.110.50.27. Redistribution subject to AIP license or copyright, see http://ojps.aip.org/phf/phfcr.jsp

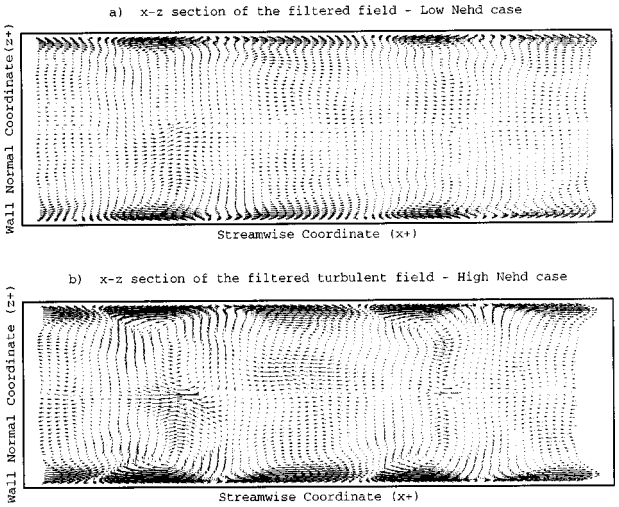

FIG. 6. Organized EHD flow field obtained by phase averaging the field and filtering out mean and turbulent components: (a) low N_{EHD}; (b) high N_{EHD}.

have been found in simulations of two-dimensional viscous flows, for N_{EHD} above a critical value of about 5. In the present work, the oscillations of the vortical cells are likely to be due also to the fluctuating character of the interactions with the turbulence field, which induce a slight dependence on time of the EHD flows. The instantaneous plots of Figs. 7(b) and 7(c), may be used to examine the modifications to the vortical cells caused by the turbulent through-flow. As N_{EHD} decreases, the initially symmetric cells upstream and downstream of the wires become different. Upstream cells

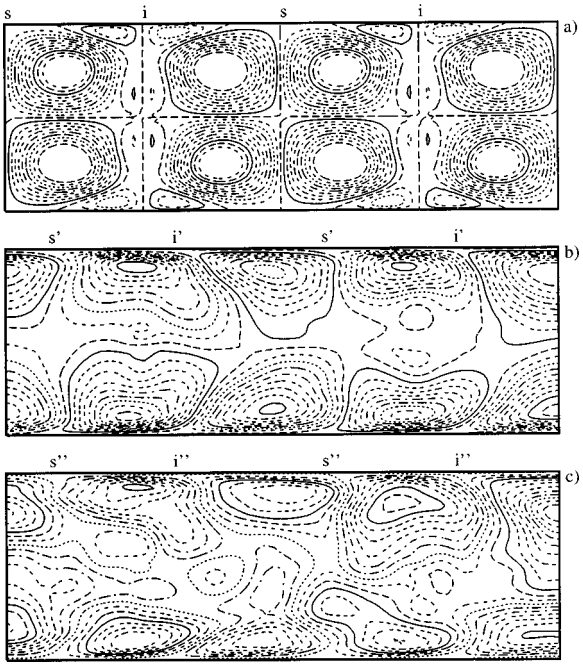

FIG. 7. Isocontours of streamlines of EHD flows in three cases: (a) $N_{\mathrm{EHD}}=\infty$, with contours going from -1 to 1 with 0.1 increments in wall units; (b) $N_{\mathrm{EHD}}=2.5$ with contours going from -0.27 to 0.3 with 0.03 increments in wall units; (c) $N_{\mathrm{EHD}}=1.1$, with contours going from -0.12 to 0.18 with 0.015 increments in wall units; Distortion of upstream and downstream vortices is uneven. Upstream flows have larger gradients but smaller extent than downstream flows.

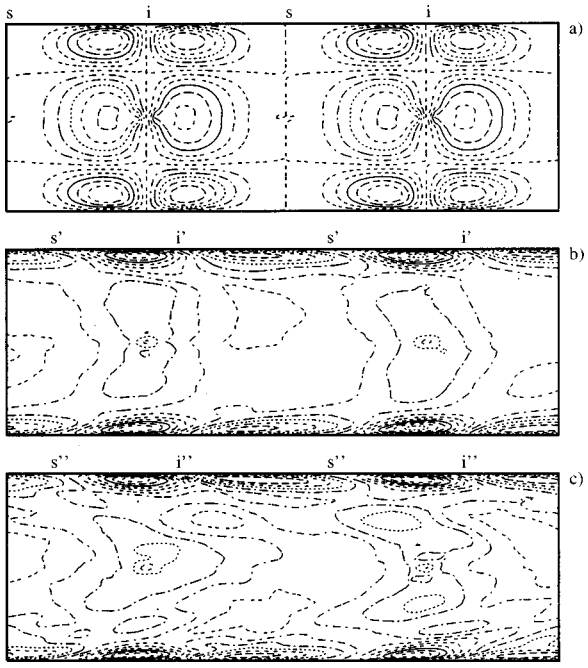

FIG. 8. Isocontours of the organized streamwise velocity component in half of channel: (a) $N_{\mathrm{EHD}}=\infty$; (b) $N_{\mathrm{EHD}}=2.5$; (c) $N_{\mathrm{EHD}}=1.1$. Lines connecting the walls are $\tilde{u}=0$ isolines. Decrease in N_{EHD} induces (i) loss of symmetry and organization; (ii) increase in the velocity gradients near the wall and their decrease in the center of channel; (iii) larger shape fluctuations. Stagnation points, located where 0 isolines touch the walls, appear advected downstream by the mean flow.

tend to assume a trapezoidal shape, while downstream cells take on a triangular shape, similar to previous findings in the viscous regime.[5,9] The upstream flows encounter an adverse pressure gradient, while downstream flows find a favorable one; therefore, the upstream branch of the upstream vortex tends to stay attached to the wall, displacing the downstream branch of the neighboring vortex from the wall. In contrast, the downstream branch of the upstream vortex is advected downstream, reducing the extent of the upstream branch of the downstream vortex, also counteracted by the stronger mean flow velocity field in the center of the channel.

Vortical cells appear also to be *squeezed* toward the wall for decreasing N_{EHD}. If N_{EHD} is reduced, the region where EHD flows can compete with the mean flow, and so maintain their identity, becomes increasingly smaller, and more confined to the wall region.

In Fig. 7(a), stagnation points are located at equally spaced intervals. The through-flow displaces the stagnation points downstream and changes the spacing between them. Two different types of stagnation points may be identified: the first (an ''i'' point) generated by impingement of the jet on the wall, and the second (an ''s'' point) generated by the return flow toward the center of the channel. Since for both types, the organized streamwise velocity component is zero, their locations are identified by the contours of the streamwise velocity component as shown in Fig. 8, in which the contour touching the walls is the zero contour. Stagnation points appear to be steady, i.e., no appreciable displacements due to turbulent fluctuations were observed. The downstream displacements of ''i'' points are 0.40 h in both high and low

Downloaded 20 Jun 2001 to 158.110.50.27. Redistribution subject to AIP license or copyright, see http://ojps.aip.org/phf/phfcr.jsp

N_{EHD} cases, whereas downstream displacements of ''s'' points are 0.62 h in the high N_{EHD} case and 0.64 h in the low N_{EHD} case. In the no-flow case, the vortical cells are 1.57 h wide. When the turbulent through-flow is imposed, the upstream vortex is $\sim 1.34\,h$ in streamwise extent, whereas the downstream vortex is about a third larger, being about 1.80 h in extent. For the N_{EHD} numbers investigated, there are no significant differences in the dimensions of the vortical cells in the low and high N_{EHD} cases.

It is clear that the through-flow reduces the intensity of EHD flows. In our simulations, the maximum wall-normal velocity (found in the wire section of the no-flow case and slightly downstream in the through-flow cases) decreases from about 0.95 m/s down to 0.11 m/s for the conditions of the high N_{EHD} case, and from about 0.45 m/s to approximately 0.04 m/s for the conditions of the low N_{EHD} case, a reduction of about an order of magnitude. The maximum value of the streamwise velocity is reduced by less, falling from 0.8 m/s to 0.34 m/s, for the high N_{EHD} case, and from 0.38 m/s to 0.15 m/s for the low N_{EHD} case. The maximum values of the streamwise component are found in the upstream branch of the upstream vortical cell.

In order to validate these findings, qualitatively comparisons were made with experimental data. The Reynolds numbers of the simulations were necessarily lower due to computer resources. For instance, experimental data of Kallio and Stock,[15] who measured the velocity of the EHD jets toward the walls were obtained in a three-wire precipitator 20.32 cm wide, with a wire-to-wire spacing of 20.32 cm. For an applied voltage of 42 000 V, the linear current density was $I = 0.5 \cdot 10^{-3}$ A/m, which, in their experiments with mean flow velocity of 1 m/s, gives $N_{EHD} \simeq 2.5$. Kallio and Stock[15] presented results for the time-averaged wall-normal velocity of the particle seeds in the section corresponding to a wire, and in that corresponding to the midpoint between two wires. Since they also provided an estimate of the Coulomb drift of particle seeds, it is possible to compare their findings against our simulation for the high N_{EHD} case. However, the Reynolds number based on mean flow velocity and duct width was more than 12 000 for their experiments—about four times larger than ours—and since their precipitator was larger than ours, their EHD structures were stronger than those obtained in the present work. Therefore, the results of our solution can be compared against their experimental data only on a qualitative basis.

In Fig. 9, where velocity has dimensions of meters per second, data are compared against the time average of the EHD organized component in the high N_{EHD} case. Figure 9(a) refers to the streamwise section, corresponding to the wire and Fig. 9(b) corresponds to the midpoint between two wires. Although there are significant differences between experimental data and the present simulation, the qualitative behavior of the velocity field in the EHD structures is similar.

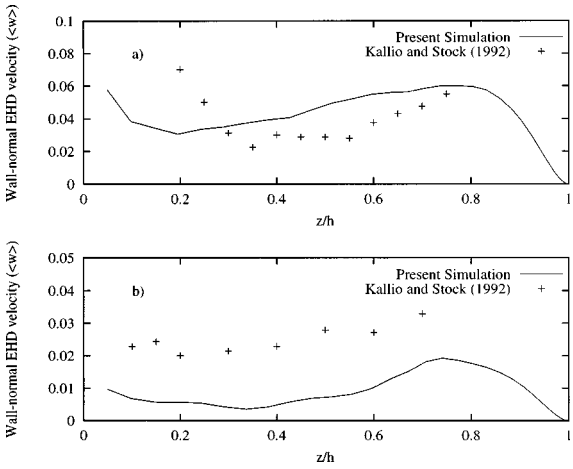

FIG. 9. Comparison of profiles of organized wall-normal component of EHD flows from the present simulations against data by Kallio and Stock (Ref. 15): (a) cross section corresponding to wire; (b) cross section corresponding to midpoint between two wires. Velocity is measured in m/s.

E. Instantaneous turbulence field

In has been shown that EHD flows reach their maximum velocity in the wall region in the streamwise direction. Filtering out the organized component clarifies the characteristics of the turbulent wall layer. If the organized component is eliminated from the overall streamwise velocity fluctuations relative to the mean shown in Figs. 5(b) and 5(c), then the fluctuating fields shown in Figs. 10(a) and 10(b) are obtained. In the low N_{EHD} case shown in Fig. 10(a), streaky structures appear that are similar to those shown in Fig. 5 for channel flow. In the high N_{EHD} case, the influence of EHD flows appears more significant though the qualitative characteristics of the reference channel flow are still there. Examination of several wall parallel sections at different times gave a spanwise spacing of the low-speed streaks of about 105 ± 15 in wall units.

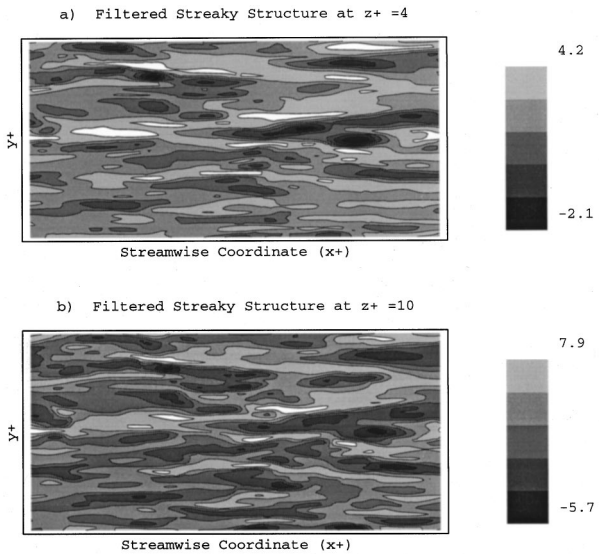

FIG. 10. Wall parallel $(x-y)$ section taken at $z^+ = 4$ of streamwise velocity component of fluctuating field. Streaky structures filtered from organized component: (a) low N_{EHD}; (b) high N_{EHD}. The shading indicates the values of the dimensionless streamwise component of the velocity field in wall units.

Downloaded 20 Jun 2001 to 158.110.50.27. Redistribution subject to AIP license or copyright, see http://ojps.aip.org/phf/phfcr.jsp

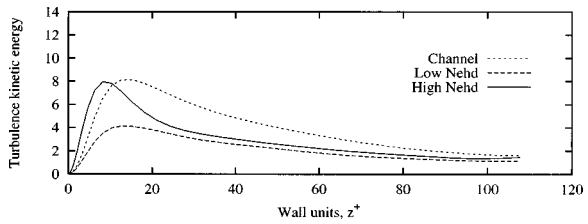

FIG. 11. Total kinetic energy of turbulence for channel flow, low N_{EHD}, and high N_{EHD}. A marked reduction in turbulence intensity is observed in low N_{EHD} case. In high N_{EHD} case, turbulence intensity is reduced in the center of the channel and increased in the wall region.

F. Statistics of the turbulence field

The filtered statistics of the turbulent velocity field give information on the distribution and intensity of turbulent fluctuations. In Fig. 11, the distribution of turbulence kinetic energy is shown for the two N_{EHD} cases and compared to that of channel flow. Consider first the low N_{EHD} case; it appears that turbulence is damped across the whole channel width. The peak is about one-half of that in channel turbulence. Examining the high N_{EHD} case, turbulence is reduced in the central region of the channel, but appears to have increased in the wall region. The position of the peak is also displaced toward the wall for increasing N_{EHD}, reducing the thickness of the wall region, and increasing the gradients. This indicates that, on the one hand, EHD flows have a damping effect on turbulence, and on the other, they introduce mechanisms that may generate turbulence in the wall region. The effects of EHD flows on turbulence intensity may be better appreciated in Fig. 12, where the rms values of the velocity fluctuations in all three directions are shown. Turbulence intensity decreases in all directions in the low N_{EHD} case. With increasing N_{EHD}, turbulence intensity increases in the streamwise direction and in the wall-normal direction. It is clear that EHD flows exert a damping action on turbulence at low N_{EHD}, but they also promote turbulence generation, an effect which becomes important at higher N_{EHD}. As we will see later, this does not mean, however, that the Reynolds stress, $-\overline{u'w'}$, increases for the high N_{EHD} case.

More information on distribution of the fluctuations in the turbulent field may be obtained by examining skewness and flatness factors, shown in Figs. 13(a)–13(f). In Figure 13(a)–13(c), the skewness factor for the fluctuations is shown for the three velocity components. A high positive value of the skewness means that velocity fluctuations more frequently attain large positive rather than negative values, and of course the reverse for negative skewness. For the streamwise component in Fig. 13(a), channel turbulence exhibits more frequent large positive fluctuations at the wall and more frequent large negative fluctuations in the center of the channel. The effect of EHD flow is to reduce the skewness at the wall in both low and high N_{EHD} cases, and to increase the skewness in the center of the channel. High positive fluctuations indicate *sweeps*, i.e., events that bring high speed fluid toward the wall. These also form the high shear stress regions at the wall. Thus the reduction in skewness with N_{EHD} indicates a reduction in either the number of sweeps or their intensity, both of which produce shear stress.

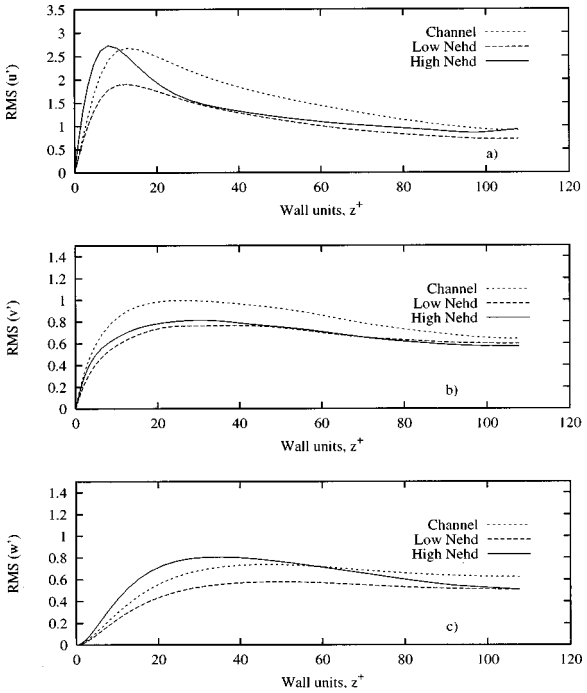

FIG. 12. Root mean square of turbulent velocity fluctuations for channel flow, low N_{EHD}, and high N_{EHD}: (a) streamwise component; (b) spanwise component; (c) wall-normal component. In the low N_{EHD} case, turbulence intensity is reduced in all directions. In the high N_{EHD} case, turbulence production by EHD flows is evident in the streamwise direction—in the wall region—and in the wall-normal direction.

Turning now to the skewness of the normal fluctuations in Fig. 13(c), it is clear that there is an increase with N_{EHD} close to the wall. A high skewness factor value is also an indicator of high rates of dissipation,[38] which will be discussed below.

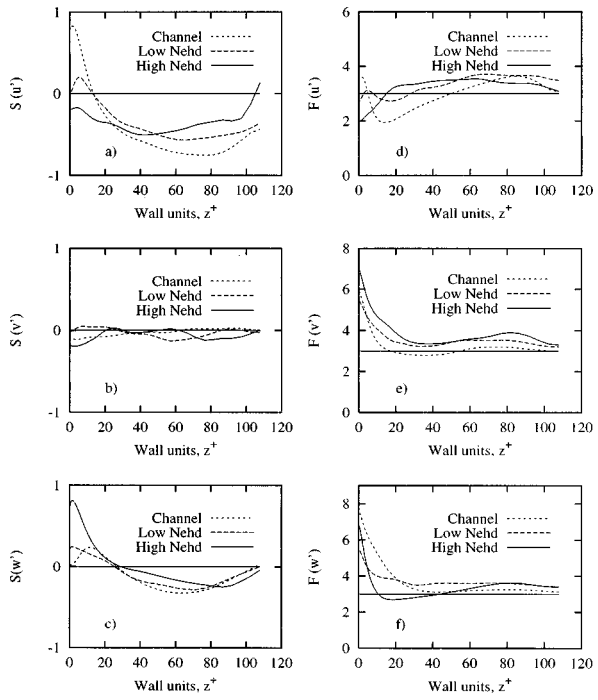

FIG. 13. Skewness and Flatness factors of turbulent velocity fluctuations for channel flow, low N_{EHD}, and high N_{EHD}: (a) Skewness factor for u'; (b) Skewness factor for v'; (c) Skewness factor for w'; (d) Flatness factor for u'; (e) Flatness factor for v'; (f) Flatness factor for w'.

Downloaded 20 Jun 2001 to 158.110.50.27. Redistribution subject to AIP license or copyright, see http://ojps.aip.org/phf/phfcr.jsp

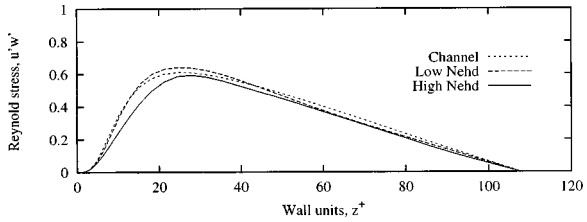

FIG. 14. Profile of Reynolds stress $-\overline{u'w'}$ filtered from organized component for channel flow, low N_{EHD}, and high N_{EHD}.

The skewness of the distribution of the spanwise fluctuating velocity, shown in Fig. 13(b), is zero everywhere, as required by symmetry considerations.

The flatness factor of the velocity fluctuations is shown in Figs. 13(d)–13(f). A *normal* distribution has a flatness factor equal to 3. A high value of the flatness factor indicates that the fluctuations are often larger than the variance of the distribution and that the fluctuations have an intermittent character. The streamwise fluctuations in Fig. 13(d) show a reduction of the flatness factor, due to the EHD effects, in proximity of the walls—more marked for increasing N_{EHD}. The flatness factor in the wall-normal direction, shown in Fig. 13(f), does not appear much influenced by the presence of EHD flows.

G. Quadrant analysis

The drag reduction caused by EHD flows as observed through the increase of the mean flow (Fig. 4) is confirmed by the behavior of the $-\overline{u'w'}$ Reynolds stress, shown in Fig. 14. In the low N_{EHD} case, the variations of the Reynolds stress are small, and mostly relative to the peak; in the high N_{EHD} case, the profile differs substantially from that of channel flow, particularly in the wall region. In the region far from the wall, all three profiles appear to collapse onto each other.

To elucidate the mechanisms by which the Reynolds stress are decreased by EHD flows, quadrant analysis[39,26] may be employed. Considering the $u'-w'$ plane, with positive w' directed outward, the Reynolds stress $-\overline{u'w'}$ is produced by four types of events: first quadrant events (I), characterized by outward motion of high-speed fluid, with $u'>0$ and $w'>0$; second quadrant events (II), characterized by outward motion of low-speed fluid, with $u'<0$ and $w'>0$, which are usually called *ejections*; third quadrant events (III), characterized by inward motion of low speed fluid, with $u'<0$ and $w'<0$; and finally, fourth quadrant events (IV), which represent motions of high-speed fluid toward the wall, with $u'>0$ and $w'<0$, and are usually called *sweeps*. Ejections and sweeps contribute to the negative Reynolds stress, i.e., to positive turbulence production, thus their increase in general corresponds to an increase of drag. First and third quadrant events contribute to positive Reynolds stress, i.e., to negative turbulence production and their increase corresponds in general to a decrease of drag. In Fig. 15, the fractional contribution of each type of event to the $-\overline{u'w'}$ Reynolds stress is presented for the low and high

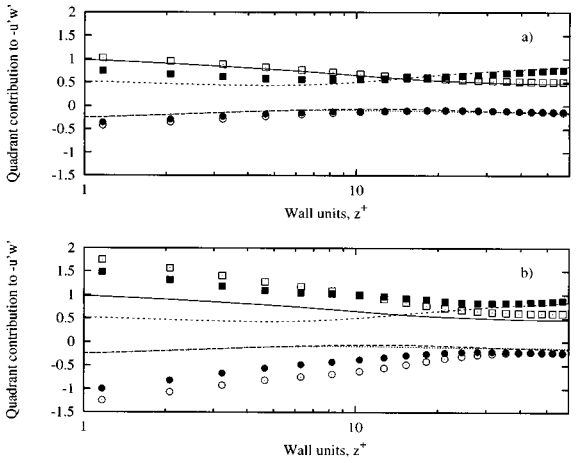

FIG. 15. Comparison of quadrant analysis for channel flow and (a) low N_{EHD}, and (b) high N_{EHD}. Lines and symbols represent the values for channel flow and channel flow with EHD effects, respectively: (●) and (– – –) first quadrant events; (□) and (– – – –) second quadrant events; (○) and (· · · ·) third quadrant events; (■) and (-----) fourth quadrant events.

N_{EHD} cases compared to channel flow. Data for channel flow are in agreement with those presented by Kim *et al.*[26] for a larger shear Reynolds number.

In channel flow, sweep events dominate close to the wall, whereas farther away ejection events dominate, with a crossover point at $z^+\simeq 12$. Contributions from first and third quadrants appear to be relatively small. The presence of EHD flows modifies the balance among the different quadrants, mostly in the wall region. They appear to increase both positive and negative Reynolds stress contributions.

At low EHD flow intensity, sweeps events are practically unaffected by EHD flows, whereas first, second, and third quadrant event contributions are all increased. At high EHD flow intensity, variations are large in all quadrants. However, the increase of the positive Reynolds stress contributions, i.e., first and third quadrants, is larger compared to that of the negative Reynolds stress contributions, i.e., second and fourth quadrants, which, coupled with the shift of the sweep/ejection crossover point closer to the wall, explains the observed drag reduction. Furthermore, analyzing the frequency of the events, we found that, in the wall region, EHD flows increase the number of first and third quadrant events, whereas they reduce the number of second and fourth quadrant events, as suggested by the behavior of the skewness of the fluctuating streamwise component.

The overall effect of EHD flows in the wall region is thus to increase the intensity of the events from all quadrants, both by increasing the intensity of the fluctuations and the correlation between streamwise and wall-normal fluctuations. However, they also affect the frequency of the different events, decreasing that of the events that give negative Reynolds stress from the second and fourth quadrants and increasing that of those that give positive Reynolds stress from first and third quadrants, and shift the sweep/ejection crossover point to reduce the sweep dominated region near the wall—thus leading to an overall reduction of the drag.

Downloaded 20 Jun 2001 to 158.110.50.27. Redistribution subject to AIP license or copyright, see http://ojps.aip.org/phf/phfcr.jsp

H. The governing equations and energy balance considerations

Insight into the dynamics of the flow field, and in particular into the mechanisms of turbulence production by EHD flows, may be gained by examining the equations of motion for each component. The continuity equation for the three fields are obtained by applying triple decomposition [Eq. (12)] to the continuity equation [Eq. (4)], and then phase-averaging, and space-averaging, over the homogeneous components. The continuity equations for all components of the flow field are

$$\frac{\partial \overline{u_i}}{\partial x_i}=\frac{\partial \tilde{u}_i}{\partial x_i}=\frac{\partial u_i'}{\partial x_i}=0. \tag{13}$$

A similar procedure is adopted for the momentum balance equations, i.e., by substituting Eq. (12) into Eq. (5), and phase averaging, we obtain the following equation,

$$\frac{\partial \tilde{u}_i}{\partial t}+\overline{u}_j\frac{\partial \overline{u_i}}{\partial x_j}+\overline{u}_j\frac{\partial \tilde{u}_i}{\partial x_j}+\tilde{u}_j\frac{\partial \overline{u_i}}{\partial x_j}+\frac{\partial}{\partial x_j}\langle u_i'u_j'\rangle+\frac{\partial}{\partial x_j}(\tilde{u}_i\tilde{u}_j)$$
$$=\frac{1}{\mathrm{Re}}\left(\frac{\partial^2\overline{u_i}}{\partial x_j\,\partial x_j}+\frac{\partial^2\tilde{u}_i}{\partial x_j\,\partial x_j}\right)-\frac{\partial \overline{p}}{\partial x_i}-\frac{\partial \tilde{p}}{\partial x_i}+\tilde{\Phi}_i, \tag{14}$$

which, averaged over the homogeneous components, gives the equation for the mean field:

$$\overline{u}_j\frac{\partial \overline{u_i}}{\partial x_j}=-\frac{\partial \overline{p}}{\partial x_i}+\frac{1}{\mathrm{Re}}\frac{\partial^2\overline{u_i}}{\partial x_j\,\partial x_j}-\frac{\partial}{\partial x_j}(\overline{u_i'u_j'})-\frac{\partial}{\partial x_j}(\overline{\tilde{u}_i\tilde{u}_j}). \tag{15}$$

As expected, there is no direct generation of mean flow by the body forces. The equation of motion for the organized EHD flows is obtained by subtracting Eq. (15) from Eq. (14). Therefore,

$$\frac{\partial \tilde{u}_i}{\partial t}+\overline{u}_j\frac{\partial \tilde{u}_i}{\partial x_j}+\tilde{u}_j\frac{\partial \overline{u_i}}{\partial x_j}$$
$$=-\frac{\partial \tilde{p}}{\partial x_i}+\frac{1}{\mathrm{Re}}\frac{\partial^2\tilde{u}_i}{\partial x_j\,\partial x_j}+\frac{\partial}{\partial x_j}(\overline{\tilde{u}_i\tilde{u}_j}-\tilde{u}_i\tilde{u}_j)$$
$$+\frac{\partial}{\partial x_j}(\overline{u_i'u_j'}-\langle u_i'u_j'\rangle)+\tilde{\Phi}_i. \tag{16}$$

In this equation, the term $\tilde{\Phi}$ is the electrostatic body force which drives the EHD flows (it is clear that $\tilde{\Phi}=\Phi$). The equation for the turbulent component of the flow field is obtained by subtracting Eq. (14) from Eq. (5). This gives

$$\frac{\partial u_i'}{\partial t}+\overline{u}_j\frac{\partial u_i'}{\partial x_j}+u_j'\frac{\partial \overline{u_i}}{\partial x_j}+\tilde{u}_j\frac{\partial u_i'}{\partial x_j}+u_j'\frac{\partial \tilde{u}_i}{\partial x_j}$$
$$=-\frac{\partial p'}{\partial x_i}+\frac{1}{\mathrm{Re}}\frac{\partial^2 u_i'}{\partial x_j\,\partial x_j}+\frac{\partial}{\partial x_j}(\langle u_i'u_j'\rangle-u_i'u_j'). \tag{17}$$

The term $-\overline{\tilde{u}_i\tilde{u}_j}$ is the organized Reynolds stress (or the EHD supported stress), appearing both in the equation for the mean field and for the organized motion. It represents the contribution of the organized flows to the transport of mean momentum. Analogously, the term $-\overline{u_i'u_j'}$ represents the contribution of the turbulence field to the mean momentum transport. Following Hussain,[37] the momentum transport due to the turbulent field, $r_{ij}'=-u_i'u_j'$, may be viewed as:

$$r_{ij}'=\overline{r}_{ij}+\tilde{r}_{ij}+r_{ij},$$

where

$$\overline{r}_{ij}=-\overline{u_i'u_j'},$$

$$\tilde{r}_{ij}=-\langle u_i'u_j'\rangle+\overline{u_i'u_j'},$$

$$r_{ij}=-u_i'u_j'+\langle u_i'u_j'\rangle.$$

These terms represent the contribution of the turbulent field to the momentum transport of the three fields: $\overline{r}_{ij}$ is the turbulent contribution to the mean momentum transport; $\tilde{r}_{ij}$ is the turbulent contribution to the organized momentum transport; and r_{ij} is the turbulent contribution to the turbulent momentum transport. In particular, $\tilde{r}_{ij}$ is the difference between the phase and space averages of the turbulent Reynolds stress, and can be interpreted as the oscillation of the turbulent Reynolds stress due to the presence of the periodic pattern.

A detailed examination of the Reynolds stress transport equation for the mean field, for the organized field and for the turbulent field are currently under investigation[40] and will be presented in a later paper. We will now examine the energy fluxes which couple the three fields through analysis of the kinetic energy transport equations.

On application of Eq. (12), the total kinetic energy, $1/2\overline{u_iu_i}$, may be expressed as the sum of the kinetic energy associated with the mean field, that associated with the organized motions and that associated with the turbulence field as

$$\tfrac{1}{2}\overline{u_iu_i}=\tfrac{1}{2}\overline{u}_i\overline{u}_i+\tfrac{1}{2}\overline{\tilde{u}_i\tilde{u}_i}+\tfrac{1}{2}\overline{u_i'u_i'}.$$

By multiplying the momentum equation for $\overline{u}_i$ [Eq. (15)], by $\overline{u}_i$, phase averaging and averaging over the homogeneous directions, we obtain the mean field kinetic energy transport equation:

$$\frac{\bar{D}}{Dt}\left(\frac{1}{2}\bar{u}_i\bar{u}_i\right)=-\frac{\partial}{\partial x_j}(\overline{p}\overline{u}_j)\underbrace{-(-\overline{u_i'u_j'})\frac{\partial \bar{u}_i}{\partial x_j}}_{\mathrm{I}}$$
$$\underbrace{-(-\overline{\tilde{u}_i\tilde{u}_j})\frac{\partial \bar{u}_i}{\partial x_j}}_{\mathrm{II}}-\frac{\partial}{\partial x_j}[\bar{u}_i(\overline{u_i'u_j'}+\overline{\tilde{u}_i\tilde{u}_j})]$$
$$+\frac{1}{\mathrm{Re}}\frac{\partial^2}{\partial x_j^2}\left(\frac{1}{2}\bar{u}_i\bar{u}_i\right)-\frac{1}{\mathrm{Re}}\frac{\partial \bar{u}_i}{\partial x_j}\frac{\partial \bar{u}_i}{\partial x_j}. \tag{18}$$

Analogously, by multiplying the momentum equation for $\tilde{u}_i$ [Eq. (16)] by $\tilde{u}_i$, phase averaging and averaging over the homogeneous directions, we obtain the organized field kinetic energy transport equation:

Downloaded 20 Jun 2001 to 158.110.50.27. Redistribution subject to AIP license or copyright, see http://ojps.aip.org/phf/phfcr.jsp

$$\frac{\bar{D}}{Dt}\left(\frac{1}{2}\overline{\tilde{u}_i\tilde{u}_i}\right)=-\frac{\partial}{\partial x_j}\left[\overline{\tilde{u}_j\left(\tilde{p}+\frac{1}{2}\tilde{u}_i\tilde{u}_i\right)}\right]+\underbrace{(-\overline{\tilde{u}_i\tilde{u}_j})\frac{\partial\bar{u}_i}{\partial x_j}}_{\text{II}}$$
$$\underbrace{-\overline{(-\langle u_i'u_j'\rangle)\frac{\partial\tilde{u}_i}{\partial x_j}}}_{\text{III}}-\frac{\partial}{\partial x_j}(\overline{\tilde{u}_i\langle u_i'u_j'\rangle})$$
$$+\frac{1}{\mathrm{Re}}\frac{\partial^2}{\partial x_j^2}\left(\frac{1}{2}\overline{\tilde{u}_i\tilde{u}_i}\right)-\frac{1}{\mathrm{Re}}\overline{\frac{\partial\tilde{u}_i}{\partial x_j}\frac{\partial\tilde{u}_i}{\partial x_j}}+\overline{\tilde{u}_i\tilde{\Phi}_i}. \tag{19}$$

Finally, by multiplying the momentum equation for u_i' [Eq. (17)] by u_i', phase averaging and averaging over the homogeneous directions, the turbulence field kinetic energy transport equation is obtained:

$$\frac{\bar{D}}{Dt}\left(\frac{1}{2}\overline{u_i'u_i'}\right)=-\frac{\partial}{\partial x_j}\left[\overline{u_j'\left(p'+\frac{1}{2}u_i'u_i'\right)}\right]+\underbrace{(-\overline{u_i'u_j'})\frac{\partial\bar{u}_i}{\partial x_j}}_{\text{I}}$$
$$\underbrace{+\overline{(-\langle u_i'u_j'\rangle)\frac{\partial\tilde{u}_i}{\partial x_j}}}_{\text{III}}+-\overline{\tilde{u}_j\frac{\partial}{\partial x_j}\left\langle\frac{1}{2}u_i'u_i'\right\rangle}$$
$$+\frac{1}{\mathrm{Re}}\frac{\partial^2}{\partial x_j^2}\left(\frac{1}{2}\overline{u_i'u_i'}\right)-\frac{1}{\mathrm{Re}}\overline{\frac{\partial u_i'}{\partial x_j}\frac{\partial u_i'}{\partial x_j}}. \tag{20}$$

In Eqs. (18), (19), and (20), the l.h.s. is the material rate of change of the mean, organized, and turbulent kinetic energy, respectively. This term is zero in steady flows. The energy from the electrostatic body force field which produces the EHD flows is the last term of Eq. (19), $\overline{\tilde{u}_i\tilde{\Phi}_i}$. The terms identified as I, II, and III are the energy fluxes that couple the three fields. Term I is the production of turbulence by the action of the turbulent Reynolds stresses against the mean strain rate. This term appears as a drain term in Eq. (18) and as a source term in Eq. (20). Analogously, term II is the production of disturbance energy by action of the mean field, through the mean strain rate, against the organized flow Reynolds stresses. This term drains energy from the mean field toward the organized field. The energy coupling between the turbulent field and the organized field is given by term III, which is the turbulent kinetic energy produced by the organized EHD flows through the phase-averaged turbulent Reynolds stresses. Term III appears as a source of turbulent kinetic energy in q. (20).

I. Turbulence kinetic energy budget

As pointed out by Hunt,[41] the direct effect of the body-force field on the kinetic energy of turbulence is zero. However, this force has a significant indirect effect on the turbulence kinetic energy budget. To analyze in detail the effect of EHD flows on transfer and production of turbulence kinetic energy, we will rewrite Eq. (20) in the following form:

$$0=-\overline{u_i'u_j'}\frac{\partial\bar{u}_i}{\partial x_j}-\frac{1}{\mathrm{Re}}\overline{\frac{\partial u_i'}{\partial x_j}\frac{\partial u_i'}{\partial x_j}}+\overline{p'\frac{\partial u_j'}{\partial x_j}}$$
$$+\frac{\partial}{\partial x_j}\overline{\left(u_j'\frac{1}{2}u_i'u_i'\right)}+\frac{1}{\mathrm{Re}}\frac{\partial^2}{\partial x_j^2}\left(\frac{1}{2}\overline{u_i'u_i'}\right)$$
$$-\frac{\partial}{\partial x_j}\overline{p'\delta_{ij}u_j'}+\underbrace{\overline{(-\langle u_i'u_j'\rangle)\frac{\partial\tilde{u}_i}{\partial x_j}}}_{P_{\mathrm{EHD}}}-\underbrace{\overline{\tilde{u}_j\frac{\partial}{\partial x_j}\left\langle\frac{1}{2}u_i'u_i'\right\rangle}}_{T_{\mathrm{EHD}}}. \tag{21}$$

The terms on the r.h.s. represent: production by mean flow, dissipation, pressure-strain correlation, turbulent diffusion, viscous diffusion, pressure diffusion, production by EHD flows (P_{EHD}), and transport by EHD flows (T_{EHD}), respectively. In the absence of EHD flows—i.e., in turbulent channel flow—the last two terms are obviously zero. The third, fourth, fifth, sixth, and eighth terms contribute to the energy transfer to other flow regions, and their integral over the flow domain is zero. Production by the mean flow, and by EHD flows, are the energy gain terms, and dissipation is the energy loss term. All terms included in Eq. (21) are normalized by u_τ^4/ν and are shown in Fig. 16 except for the pressure-strain term. For clarity of presentation, the EHD-related terms, P_{EHD} and T_{EHD}, have been plotted by shifting their zero by -0.2 and -0.3, in the low and high N_{EHD} cases, respectively.

Turbulence production by action of the mean flow is given by the product of the mean strain rate, $d\bar{u}/dz$, shown in Fig. 17, and $-\overline{u'w'}$, the turbulent Reynolds stress, as shown in Fig. 14. Note that the Reynolds stresses decrease with increasing N_{EHD}, consistent with the mean velocity increase with increasing N_{EHD} discussed earlier.

For the N_{EHD} examined, mean flow production is slightly increased by the presence of EHD flows.

Consider now the new term of turbulence production by EHD flows: P_{EHD} is given by the action of the phase-averaged fluctuating Reynolds stress, $-\langle u_i'u_j'\rangle$, against the organized strain rate, $\partial\tilde{u}_i/\partial x_j$. In the low N_{EHD} case, this term accounts for one fourth of total turbulence kinetic energy production, whereas in the high N_{EHD} case it has the same importance as the mean flow production term. Since $\tilde{u}_2=\partial\tilde{u}_i/\partial x_2=0$, P_{EHD} may be written as:

$$P_{\mathrm{EHD}}=-\overline{\langle u_1'u_1'\rangle\frac{\partial\tilde{u}_1}{\partial x_1}}-\overline{\langle u_1'u_3'\rangle\frac{\partial\tilde{u}_1}{\partial x_3}}-\overline{\langle u_3'u_1'\rangle\frac{\partial\tilde{u}_3}{\partial x_1}}$$
$$-\overline{\langle u_3'u_3'\rangle\frac{\partial\tilde{u}_3}{\partial x_3}}, \tag{22}$$

from which we see that turbulence kinetic energy is produced both in the streamwise and in the wall-normal direction. From Figs. 16(b) and 16(c), it may be observed that turbulence is produced mostly in the wall region. Production in the wire region is very limited. Furthermore, increasing the intensity of EHD flows displaces the peak toward the wall. Equation (22) shows that no turbulence production occurs in the spanwise component, which thus receives kinetic energy from the pressure-strain terms, which are shown in

Downloaded 20 Jun 2001 to 158.110.50.27. Redistribution subject to AIP license or copyright, see http://ojps.aip.org/phf/phfcr.jsp

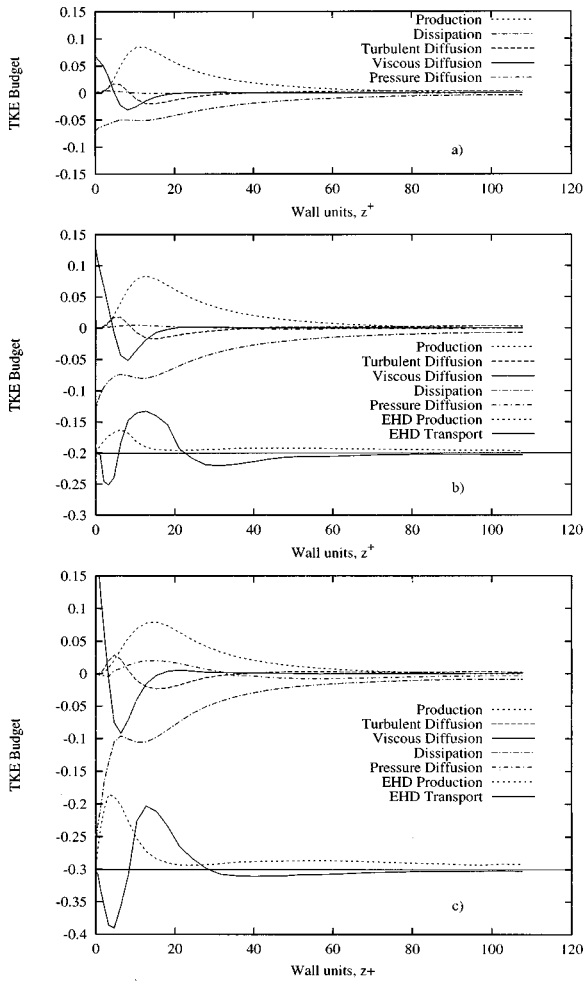

FIG. 16. Turbulent kinetic energy budget: (a) channel flow; (b) low N_{EHD}; (c) high N_{EHD}. New terms of energy input and transfer are generated by EHD flows: turbulence production by EHD flows and turbulence transfer by EHD organized motions. For clarity of presentation, the zero of these new terms is shifted by -0.2 in the low N_{EHD} case and by -0.3 in the high N_{EHD} case. All terms made dimensionless by u_τ^4/ν.

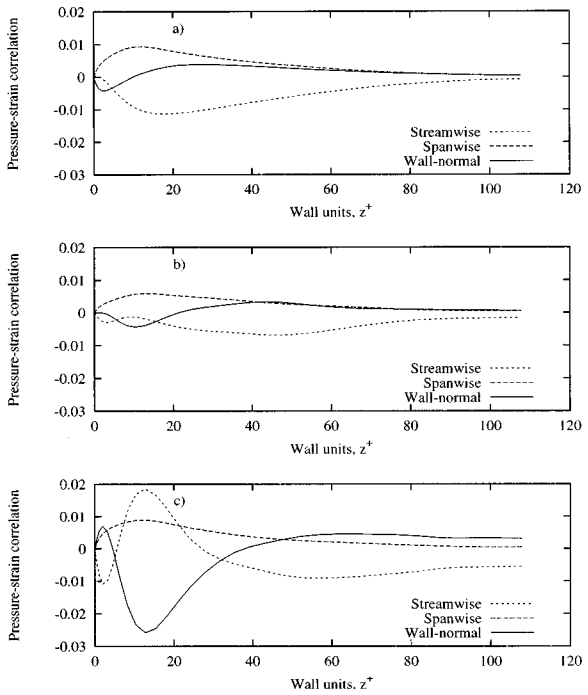

FIG. 18. Profile of pressure-strain correlation for (a) channel flow; (b) low N_{EHD}; (c) high N_{EHD}. In channel flow, turbulence kinetic energy is produced entirely in the streamwise direction. EHD flows produce turbulent kinetic energy both in wall-normal and in streamwise directions.

Fig. 18. For incompressible fluids the sum of the three pressure-strain components is always zero. Examination of each component, however, indicates how kinetic energy is transferred among the velocity components. In channel flow turbulence kinetic energy is received entirely by the streamwise component, and is redistributed to the other components. The wall-normal component becomes negative at the wall because fluctuations are damped. EHD flows modify this balance producing $(1/2)\overline{u_3'^2}$ at the edge of the wall region (around $z^+ \simeq 10$) and $(1/2)\overline{u_1'^2}$ at the wall. Finally, we can see that in the low N_{EHD} case, all pressure-strain terms are decreased. Since it can be seen from Fig. 19 that the rms of pressure fluctuations increases due to the EHD flows, it can be concluded that turbulence velocity gradients are also reduced, corresponding to a general *smoothing* of the field.

It is apparent that EHD flows increase turbulence production. However, they also increase dissipation. The peak at the wall almost doubles in the low N_{EHD} case, and increases more than three times in the high N_{EHD} case.

Turbulent diffusion, viscous diffusion and pressure diffusion are also affected by the presence of EHD flows.

Finally the EHD flows transfer term, T_{EHD}, redistributes turbulence kinetic energy to other regions by means of the organized flows. Its most significant role is to receive energy in the wall region and redistribute it farther from the wall.

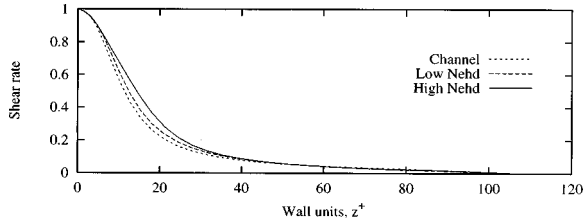

FIG. 17. Profile of shear rate in the duct for channel flow, low N_{EHD}, and high N_{EHD}.

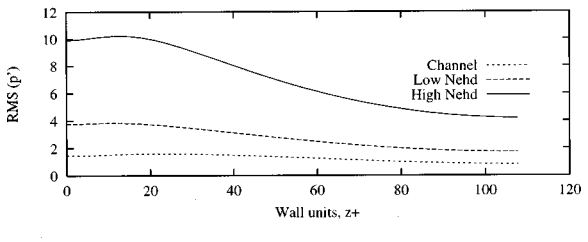

FIG. 19. Profile of the rms pressure fluctuations in channel flow, low N_{EHD}, and high N_{EHD} cases.

Downloaded 20 Jun 2001 to 158.110.50.27. Redistribution subject to AIP license or copyright, see http://ojps.aip.org/phf/phfcr.jsp

IV. SUMMARY AND CONCLUSIONS

The flow field generated by the interactions between a turbulent through-flow and spanwise EHD vortical motions is of interest in the evaluation of transport parameters in wire-plate electrostatic precipitators. Examination of the literature leads to the conclusion that theoretical work was limited to viscous flow, and numerical evaluations performed with $k-\epsilon$ models. Furthermore, experimental approaches have proven difficult because of interference caused by the electrical field. For example, the turbulence measurements by hot-wire techniques are difficult in the wire section of the precipitator, and can only be used well downstream from such regions. LDA techniques may be applied in the wire region, but measurements are biased by the drift velocity which seed particles have with respect to the flow. These problems have led to interpretations of experimental findings which sometimes contradict each other and leave the fundamental mechanisms controlling the coupling between the EHD flows and the turbulent flow field unclear.

DNS provides a clear picture of the flow field, enabling the calculation of various turbulence statistics and the examination of the instantaneous flow structure. In this work, the flow field obtained by superimposing a through turbulent channel flow onto the EHD recirculating structures in a typical wire-plate precipitator was simulated for two different intensities of the electrostatic body force characterized by the governing dimensionless number, N_{EHD}, equal to 1.1 and 2.5. These values are typical of laboratory-scale and industrial-scale facilities. The balance equations for the fluid were solved directly with a pseudo-spectral method.

The flow field was examined by decomposing it into a mean field, an organized EHD field, and a turbulence field. Using this *triple* decomposition, the modifications of the turbulence field induced by EHD flows, and the modifications of the EHD flows because of the presence of the through-flow, were isolated.

The first interesting result is that the drag is increasingly reduced with increasing EHD flow intensity. Since the numerical experiments were conducted at constant pressure drop, the observed mean velocity increased about 3% in the low N_{EHD} case and more than 6% in the high N_{EHD} case—suggesting drag reduction of about 6% and 12%, respectively. From the viewpoint of the overall energy budget of the electrostatic precipitator, drag reduction is a second order effect: the power required to drive the flow is about 23% of the overall power required to operate an ESP in the low N_{EHD} case, and about 7.5% in the high N_{EHD} case. This indicates that the overall saving is of the order of 2% in the low N_{EHD} case, and about 1% in the high N_{EHD} case.

The structure of undisturbed EHD flows is modified by the turbulent through-flow. Each wire generates two pairs of counter-rotating vortical cells, with an upstream vortex and a downstream vortex, advected downstream by the mean flow. No vortex shedding was noted. The structure of these EHD flows appeared only weakly time dependent, with the stagnation points at the walls observed to be steady. Because of the adverse pressure gradient, upstream flow branches tended to be shorter than corresponding downstream flow branches, and tended to stay close to the walls. The upstream vortical cells assume a trapezoidal shape—short at the wall and long in the center of the channel—and the downstream vortical cells assume a triangular shape—long at the wall and short in the center of the channel. Maximum velocity is reached by EHD flows in the upstream branches in the wall region. In the high N_{EHD} case, the maximum velocity of the EHD flow is about one third of the mean flow velocity.

Examination of turbulence statistics indicates that the presence of EHD flows has a twofold effect; viz. they induce higher dissipation but they also increase production using their own energy. On one hand, the increased dissipation damps turbulence rather uniformly throughout the channel; on the other hand, turbulence production increases, mostly in the wall region. The balance between these two effects gives the overall effect on turbulence intensity. In the low intensity EHD flows case, turbulence is reduced if compared to the corresponding channel flow case. In the high N_{EHD} case, turbulence intensity is reduced in the center of the channel, but increases in the wall region. However, the Reynolds stress $-\overline{u'w'}$ decreases with increasing N_{EHD}, consistent with the increase in mean velocity discussed earlier. This reduction is responsible for the drag reduction observed and can be explained by a quadrant analysis of the Reynolds stresses. Increasing the intensity of EHD flows corresponds to an increase of the intensity of events from all quadrants. However, the frequency of the negative Reynolds stress contributions, i.e., ejections and sweeps, responsible for positive turbulence production, is decreased if compared to channel flow. Altogether, this causes a reduction of the Reynolds stress, particularly in the wall region. Furthermore, the sweep/ejection crossover point is shifted to reduce the sweep dominated region near the wall—all this leading to drag reduction.

The features of the turbulence field in the wall region, e.g., the streaky structures, do not appear qualitatively different due to the presence of EHD flows. Streak characteristics—spacing and length—are similar to those for channel flow.

Examination of the governing equations and of the kinetic energy balance for the mean field, for the organized field and for the turbulence field allow estimation of the energy fluxes coupling the three fields. In particular, an analysis of the turbulent kinetic energy budget was presented. EHD flows are coupled to the turbulence field by a production term, given by the action of the phase-average fluctuating Reynolds stress against the organized strain rate, and by a transport term, which transfers turbulence kinetic energy to other regions by means of the organized field. In the low N_{EHD} case, turbulence production by EHD flows is moderate and turbulence damping is the main effect. In the high N_{EHD} case, turbulence production by EHD flows is of the same significance as turbulence production by the mean flow.

Finally, it appears that modulation of the flow field through tuning N_{EHD} could improve the performance of ESPs both with regard to collection efficiency and pressure loss. The influence of EHD flows on particle transport and collection efficiency is currently being investigated.[42]

Downloaded 20 Jun 2001 to 158.110.50.27. Redistribution subject to AIP license or copyright, see http://ojps.aip.org/phf/phfcr.jsp

ACKNOWLEDGMENTS

This work was supported by CNR under Grant No. 94.01726.CT03. Computational resources provided by CINECA, Casalecchio di Reno (Bo), Italy, under Grant No. C92-T2TUDZP1 on CRAY C-92/2128, and by NCSA, Urbana-Champaign, IL, under Grant No. CBT30000N on the CRAY Y-MP4/464 for the initial stage of the project, are gratefully acknowledged.

[1] J. R. Melcher and G. I. Taylor, ''Electrohydrodynamics: a review of the role of interfacial shear stress,'' Annu. Rev. Fluid Mech. **1**, 11 (1969).
[2] A. Castellanos, ''Coulomb-driven convection in electrohydrodynamics,'' IEEE Trans. Electr. Insul. **26**, 1201 (1991).
[3] S. El-Khabiry and G. M. Colver, ''Drag reduction by dc corona discharge along an electrically conductive flat plate for small Reynolds number flow,'' Phys. Fluids **9**, 587 (1997).
[4] C. H. Crawford and G. E. Karniadakis, ''Reynolds stress analysis of EMHD-controlled wall turbulence. Part I. Streamwise forcing,'' Phys. Fluids **9**, 788 (1997).
[5] T. Yamamoto and H. R. Velkoff, ''Electrohydrodynamics in an electrostatic precipitator,'' J. Fluid Mech. **108**, 1 (1981).
[6] F. M. J. McCluskey and P. Atten, ''Modifications to the wake of a wire across Poiseuille flow due to unipolar space charge,'' J. Fluid Mech. **197**, 81 (1988).
[7] O. E. Ramadan and S. L. Soo, ''Electrohydrodynamic secondary flow,'' Phys. Fluids **39**, 1943 (1969).
[8] A. Yabe, Y. Mori, and K. Hijikata, ''EHD study of the corona wind between wire and plate electrodes,'' AIAA J. **16**, 340 (1978).
[9] F. C. Lai, P. J. McKinney, and J. H. Davidson, ''Oscillatory electrohydrodynamic gas flows,'' J. Fluids Eng. **117**, 491 (1995).
[10] EHD flows generated by a negative *tuft* ionic discharge have a three-dimensional structure, and have been speculated to have a torus or a *doughnut* like shape. See work by T. Yamamoto and L. E. Sparks, IEEE Trans. Ind. Appl. **IA-22**, 880 (1986) for further reference.
[11] G. L. Leonard, M. Mitchner, and S. A. Self, ''An experimental study of the electrohydrodynamic flow in electrostatic precipitators,'' J. Fluid Mech. **127**, 123 (1983).
[12] J. H. Davidson and E. J. Shaughnessy, ''Turbulence generation by electric body forces,'' Exp. Fluids **4**, 17 (1986).
[13] J. H. Davidson and P. J. McKinney, ''Turbulent mixing in a barbed plate-to-plate electrostatic precipitator,'' Atmos. Environ. **23**, 2093 (1989).
[14] J. H. Davidson and P. J. McKinney, ''EHD flow visualization in the wire-plate and barbed plate electrostatic precipitator,'' IEEE Trans. Ind. Appl. **27**, 154 (1991).
[15] G. A. Kallio and D. E. Stock, ''Interaction of electrostatic and fluid dynamic fields in wire-plate electrostatic precipitators,'' J. Fluid Mech. **240**, 133 (1992).
[16] S. Bernstein and C. T. Crowe, ''Interaction of electrostatics and fluid dynamics in electrostatic precipitators,'' Environment International **6**, 181 (1981).
[17] C. Riehle and F. Löffler, ''Particle dynamics in an electrohydrodynamic flow field investigated with a two-component laser-doppler velocimeter,'' Part. Part. Syst. Charact. **10**, 41 (1993).
[18] G. A. Kallio and D. E. Stock, ''Flow visualization inside a wire-plate electrostatic precipitator,'' IEEE Trans. Ind. Appl. **26**, 503 (1990).
[19] K. Lam and S. Banerjee, ''On the condition of streak formation in bounded flows,'' Phys. Fluids A **4**, 306 (1992).
[20] A. Soldati, P. Andreussi, and S. Banerjee, ''Direct simulation of turbulent particle transport in electrostatic precipitators,'' AIChE. J. **39**, 1910 (1993).
[21] A. Soldati, M. Casal, P. Andreussi, and S. Banerjee, ''Lagrangian simulation of turbulent particle dispersion in electrostatic precipitators,'' AIChE. J. **43**, 1403 (1997).
[22] G. Leutert and B. Bohlen, ''The spatial trend of electric field strength and space charge density in plate type electrostatic precipitator,'' Staub-Reinhalt Luft **32**, 27 (1972) (in English).
[23] The force actually applied to the ions is the Lorenz force: $\mathbf{F}_L = \rho_c \mathbf{E} + \mathbf{J} \times \mathbf{B}$, in which $\mathbf{J}$ is the current density vector and $\mathbf{B}$ is the local magnetic flux density field. However, since in electrostatic precipitators current densities are low, the magnetic contribution to the body force is negligible and the ionic species are subject only to the Coulomb force.
[24] J. R. Melcher, *Continuum Electromechanics* (MIT, Cambridge, 1981).
[25] B. Malraison, P. Atten, and A. T. Perez, ''Panaches chargés résultant de l'injection d'ions dans un liquide isolant par une lame ou une pointe placée en face d'un plain,'' J. Phys. III **4**, 81 (1994).
[26] J. Kim, P. Moin, and R. Moser, ''Turbulence statistics in fully developed channel flow at low Reynolds number,'' J. Fluid Mech. **177**, 133 (1987).
[27] E. W. Mc Daniel and E. A. Mason, *The Mobility and Diffusion of Ions in Gases* (Wiley, New York, 1973).
[28] J. H. Davidson, personal communication, University of Minnesota at Minneapolis, November 1997.
[29] H. Eckelmann, ''The structure of the viscous sublayer and the adjacent wall region in a turbulent channel flow,'' J. Fluid Mech. **65**, 439 (1974).
[30] H. P. Kreplin and H. Eckelmann, ''Behaviour of the fluctuating velocity components in the wall region of a turbulent channel flow,'' Phys. Fluids **22**, 1233 (1979).
[31] S. L. Lyons, T. J. Hanratty, and J. B. McLaughlin, ''Large-scale computer simulation of fully developed channel flow with heat transfer,'' Int. J. Numer. Methods Fluids **13**, 999 (1991).
[32] J. W. Brooke and T. J. Hanratty, ''Origin of turbulence-producing eddies in a channel flow,'' Phys. Fluids A **5**, 1011 (1993).
[33] S. K. Robinson, ''Coherent motions in the turbulent boundary layer,'' Annu. Rev. Fluid Mech. **23**, 601 (1991).
[34] D. Kaftori, G. Hetsroni, and S. Banerjee, ''Funnel-shaped vortical structures in wall turbulence,'' Phys. Fluids **6**, 3035 (1994).
[35] W. C. Reynolds and A. K. M. F. Hussain, ''The mechanics of an organized wave in turbulent shear flow. Part 3. Theoretical models and comparison with experiments,'' J. Fluid Mech. **54**, 263 (1972).
[36] J. A. Harris and R. L. Street, ''Numerical simulation of turbulent flow over a moving wavy boundary: Norris and Reynolds extended,'' Phys. Fluids **6**, 924 (1994).
[37] A. K. M. F. Hussain, ''Coherent structures—Reality and myth,'' Phys. Fluids **26**, 2816 (1983); ''Coherent structures and turbulence,'' J. Fluid Mech. **173**, 303 (1986).
[38] A. A. Townsend, *The Structure of Turbulent Shear Flow* (Cambridge University Press, Cambridge, 1976).
[39] J. M. Wallace, H. Eckelmann, and R. S. Brodkey, ''The wall region in turbulent shear flow,'' J. Fluid Mech. **54**, 39 (1972).
[40] A. Soldati and S. Banerjee, ''Drag reduction mechanisms in a turbulent Poiseuille flow with superimposed EHD structures,'' Bull. Am. Phys. Soc. **42**, 2247 (1997).
[41] J. C. R. Hunt, ''Effects of body forces on turbulence,'' in *Advances in Turbulence V*, edited by V. R. Benzi (Kluwer, Dordrecht (NL), 1995), p. 229.
[42] A. Soldati and S. Banerjee, ''Influence of electrohydrodynamics on turbulent particle transport in electrostatic precipitators,'' AIChE Annual Meeting, Chicago, Nov. 18–21, 1996.

Downloaded 20 Jun 2001 to 158.110.50.27. Redistribution subject to AIP license or copyright, see http://ojps.aip.org/phf/phfcr.jsp